Optics Letters

Graphene–metal hybrid metamaterials for strong and tunable circular dichroism generation

Zhong Huang,[1,2] Kan Yao,[3] Guangxu Su,[1] Wei Ma,[2] Lin Li,[2] Yongmin Liu,[2,3,4] Peng Zhan,[1,*] and Zhenlin Wang[1,5]

[1]School of Physics and National Laboratory of Solid State Microstructures, Nanjing University, Nanjing 210093, China
[2]Department of Mechanical and Industrial Engineering, Northeastern University, Boston, Massachusetts 02115, USA
[3]Department of Electrical and Computer Engineering, Northeastern University, Boston, Massachusetts 02115, USA
[4]e-mail: y.liu@northeastern.edu
[5]e-mail: zlwang@nju.edu.cn
*Corresponding author: zhanpeng@nju.edu.cn

Received 2 March 2018; accepted 23 April 2018; posted 2 May 2018 (Doc. ID 325105); published 29 May 2018

A strong and dynamically controlled circular dichroism (CD) effect has aroused great attention due to its desirable applications in modern chemistry and life sciences. In this Letter, we propose a graphene–metal hybrid chiral metamaterial to generate mid-infrared CD with an intensity of more than 10%, which can be actively controlled over a wide wavelength range. In addition to the strong tunability, the CD signal intensity of our nanostructure is drastically larger than that of the purely graphene-based chiroptical nanostructures. Our design offers a new strategy for developing tunable chiral metadevices, which could be used in various applications, such as biochemical detection and information processing.

OCIS codes: (160.3918) Metamaterials; (160.1585) Chiral media.

https://doi.org/10.1364/OL.43.002636

Chirality refers to a certain handedness in three-dimensional (3D) geometry without any mirror symmetry plane [1], which is important in chemistry and life sciences because different chiral molecules can lead to distinctly different physiological responses. For a chiral medium subject to the illumination of right-handed circularly polarized (RCP) or left-handed circularly polarized (LCP) light, different optical responses, including selective transmission/reflection and circular dichroism (CD), occur. For example, gyroid nanostructures produce the vivid colors of butterfly wings [2], and Chrysina gloriosa under LCP illumination appear more brilliant than those under RCP illumination [3]. Other species, such as DNA double helix, sugar, cholesteric liquid crystals, and some biomolecules are all 3D chiral structures existing in nature. However, the chiroptical response in natural materials is generally very weak due to the small electromagnetic interaction volume [4]. Consequently, the CD effect is detectable only when the optical path length is much larger than the wavelength of light, which limits its further applications at the nanoscale.

Surface plasmons (SPs), electromagnetic modes existing at a metal–dielectric interface, present unique advantages in supporting sub-diffraction-limited spatial light confinement and a strongly enhanced local electric field [5], which can significantly improve the strength of light–matter interactions [6]. Recent progress in plasmonics paves the way for the enhancement of the CD effect [7–9]. To date, the CD effects of 3D metallic nanostructures have been widely investigated [10] and applied in various fields, such as chiral catalysis [11], biological monitoring [12], polarization tuning [13], and chiral photo detection [14]. In these cases, the giant CD signals were attributed to the large light–matter interaction owing to the excitation of the electric and magnetic resonant modes [15]. Nevertheless, due to the restricted flexibility of the permittivity of noble metals, CD effects normally occur at a narrow band. In addition, it is very difficult to change the geometrical parameters of the structure after fabrication. Hence, more appropriate materials are highly desirable for dynamically and precisely manipulating the CD effects.

Graphene, a monolayer of carbon atoms gathered in a honeycomb lattice, has attracted significant attention since it provides unique opto-electric properties beneficial for electronic [16], structural [17], and transport applications [18]. As it supports SPs with both high confinement and relatively low loss [19], so far, graphene has been extensively studied for applications in plasmonic waveguides [20], absorbers [21], and wide-range tunable metamaterials [22–24] in the infrared and terahertz spectral ranges. Moreover, by electrical gating, graphene shows great tunability of its electromagnetic properties via changing its surface conductivity [20]. With these advantages, graphene is considered as a promising candidate for actively tunable plasmonic CD nanostructures. Graphene-based split-ring [25] and nanodisk [26] arrays were proposed to generate tunable CD signals, and mid-infrared circular conversion dichroism also could be tuned by integrating a monolayer graphene film with metallic nanostructures [27]. Although the tuning range is broad, the CD signals from purely graphene-based nanostructures are too small to be applied in practice because of the weak near-field coupling and small electromagnetic interaction volume determined by the nature of graphene [18].

Thus, it is compelling to exploit novel approaches to actively control the CD signal while maintaining a relatively large value of CD.

In this Letter, we present a new design of chiral metamaterial, which is devised to break mirror symmetries [8,9] to generate a tunable and strong CD effect based on a bi-layer hybrid nanostructure composed of gold split-ring resonators (SRRs) and graphene gratings. We utilize the electromagnetically induced transparency (EIT) effect of this system arising from the destructive interference between the metallic SRR's magnetic resonance and graphene's electric resonance, which dramatically increases the light–matter interaction time and volume [28] and, consequently, leads to a strong narrow-band CD effect. As a proof-of-concept, a large CD targeted at ~8.25 μm with a value of up to 13% is achieved, which is significantly larger than the CD of 4% achieved by pure graphene chiral metamaterials [25,26]. To further clarify the underlying physics of the enhanced CD effect, a theoretical analysis based on the coupled-mode theory (CMT) [29,30] is applied, and the modeled results show excellent agreement with numerical simulations. The active control of the CD effect is demonstrated by tuning the Fermi energy of graphene via changing the gate voltage, the geometrical parameters, and the environmental dielectric constants. In the broad mid-infrared regime of our interest from 6 to 10 μm, the CD value remarkably maintains greater than 10%. Our results could be useful for vibrational CD spectroscopy in the mid-infrared region to determine the configuration of a chiral molecule.

The schematic of the proposed chiral metamaterial is shown in Fig. 1(a). The unit cell is composed of a graphene strip at the bottom layer and a gold SRR at the top layer. The graphene strip lies along the y-direction, and the SRR is right above (along the positive z-direction) the graphene. The vertical distance (d) between the SRR and the graphene is 0.5 μm, and the thickness of the SRR is 30 nm. The whole structure is excited by a normally incident RCP or LCP plane wave. Here RCP or LCP is defined if the electric field vector rotates clockwise (counterclockwise) when an observer looks along the wave propagation direction [8]. Figure 1(b) displays the detailed parameters of a unit cell of the metamaterial (top view). The array periodicities p along the x- and y-directions are identical and set as 4 μm. The arm length of the SRR (l) is 1.6 μm, and the arm width (w) is 0.4 μm. The width of the graphene grating (w_g) is 230 nm. The SRR is rotated about the z-axis by an angle $\theta = 45°$ and, thus, the mirror symmetry of the system is broken, fulfilling the necessary condition to generate CD [8,9]. These geometrical parameters have been optimized using full-wave numerical simulations based on COMSOL. In our simulations, the permittivity of gold is described by the Drude model, $\varepsilon_{\text{gold}} = 1 - \omega_p^2/(\omega(\omega + i\Gamma))$, where $\omega_p = 1.37 \times 10^{16}$ s^{-1} is the plasma frequency, and $\Gamma = 4.08 \times 10^{13}$ s^{-1} is the damping constant, respectively [28]. For monolayer graphene, the thickness (t_g) is assumed to be 0.5 nm [21], and its permittivity can be derived from $\varepsilon_g = \varepsilon_0 + i\sigma_g/(\omega t_g)$ with ε_0 the dielectric constant of the vacuum. Here σ_g represents the complex surface conductivity of graphene, which involves contributions from the intra- and inter-band transitions and can be calculated through the local limit of random-phase approximation [21]. The whole structure is embedded in a homogeneous dielectric medium with a dielectric constant ε_d to make the interface effect negligible. For simplicity, the dielectric environment is considered as air with $\varepsilon_d = 1$.

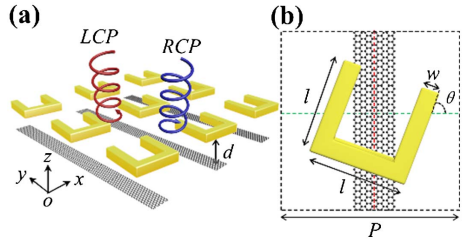

Fig. 1. (a) 3D schematic view of the chiral metamaterial. (b) Top view of a unit cell.

To have a clear physical insight into our proposed metamaterial, the CMT is applied to investigate the CD effect since both the graphene strip and the SRR experience dissipation, as well as near-field coupling. In the linear polarization basis, the transmission matrix is defined by $T_{\text{lin}}\vec{a} = \vec{b}$, where $\vec{a} = [a_x, a_y]^T$ are the amplitudes of the incident plane waves, $\vec{b} = [b_x, b_y]^T$ are the transmitted wave amplitudes, and the subscript x (y) denotes the linear polarization direction. The transmission matrix can be re-expressed in the circular polarization basis by using the basis vectors $(1, +i)^T/\sqrt{2}$ (LCP) and $(1, -i)^T/\sqrt{2}$ (RCP). The result is as follows:

$$T_{\text{circ}} = \begin{pmatrix} t_{RR} & t_{LR} \\ t_{RL} & t_{LL} \end{pmatrix}, \tag{1}$$

in which

$$t_{RR} = 0.5[(t_{xx} + t_{yy}) + i(t_{xy} - t_{yx})], \tag{2a}$$

$$t_{LR} = 0.5[(t_{xx} - t_{yy}) - i(t_{xy} + t_{yx})], \tag{2b}$$

$$t_{RL} = 0.5[(t_{xx} - t_{yy}) + i(t_{xy} + t_{yx})], \tag{2c}$$

$$t_{LL} = 0.5[(t_{xx} + t_{yy}) - i(t_{xy} - t_{yx})], \tag{2d}$$

where t_{xx}, t_{xy}, t_{yx}, and t_{yy} denote the matrix elements of T_{lin}.

Let $\vec{q} = [q_x, q_y]^T$ represent the complex oscillation amplitudes for the resonances (the graphene strip and the SRR) oriented in the x and y directions. The incident light (described by $\vec{a}$) couples linearly to both resonators, according to the coupled-mode equation:

$$\Omega\vec{q} = K\vec{a}, \tag{3}$$

for the 2×2 complex matrices Ω and K. Moreover, the outgoing light (described by $\vec{b}$) is a combination of the direct transmission of the inputs and the re-radiation by the resonators:

$$\vec{b} = K^T\vec{q} + Ia. \tag{4}$$

The Ω and K matrices can be parametrized by

$$\Omega = \begin{pmatrix} -i\delta_x - (\gamma_x^s + \gamma_x^d) & i\kappa \\ i\kappa & -i\delta_y - (\gamma_y^s + \gamma_y^d) \end{pmatrix}, \tag{5}$$

where $\delta_\mu (\mu = x, y)$ is the frequency detuning for each resonator, γ_μ^s is the radiative scattering rate, γ_μ^d is the dissipation rate, and κ is the near-field coupling rate. The transmission matrix then takes the form

$$T_{\text{lin}} = I + K^T\Omega^{-1}K, \tag{6}$$

while Eqs. (2a) and (2d) can be expressed in terms of the CMT parameters:

$$t_{RR} = 0.5\left[\frac{\gamma_1^d\gamma_2^s - 2\kappa\sqrt{\gamma_1^s\gamma_2^s} - \gamma_1^s\gamma_2^d - i(\delta_1\gamma_2^s + \delta_2\gamma_1^s)}{\kappa^2 + (-i\delta_2 - \gamma_2^d - \gamma_2^s)(-i\delta_1 - \gamma_1^d - \gamma_1^s)}\right]$$

$$t_{LL} = 0.5\left[\frac{\gamma_1^d\gamma_2^s + 2\kappa\sqrt{\gamma_1^s\gamma_2^s} - \gamma_1^s\gamma_2^d - i(\delta_1\gamma_2^s + \delta_2\gamma_1^s)}{\kappa^2 + (-i\delta_2 - \gamma_2^d - \gamma_2^s)(-i\delta_1 - \gamma_1^d - \gamma_1^s)}\right]. \quad (7)$$

In order to demonstrate the formation mechanism of the CD effect clearly, we first study the transmission spectra under the normal incidence of circularly polarized light (CPL) for the graphene grating only and the gold SRR only, as shown in Figs. 2(a) and 2(c), respectively. For the optimized structural parameters mentioned above, a transmission dip of the graphene grating with a narrow linewidth centered at ~8.45 μm is evidenced in Fig. 2(a), which arises from the excitation of a coupled electric dipole resonant mode recognized by the normalized electric field distribution ($|E/E_{in}|^2$), as illustrated in Fig. 2(b). As a comparison, the full-wave COMSOL simulation results are marked as red circles in the same plot in Fig. 2(a), which agree perfectly with the calculation from the CMT. Here the graphene's Femi energy (E_f) and electron mobility (μ) are 0.8 eV and 10,000 cm^2/Vs, respectively. It is obvious that a strongly localized electric field is concentrated firmly at the edges of the graphene grating with an enhancement of ~1.8×10^4. On the other hand, for the SRR alone, a broad transmission dip centered at ~8.25 μm is observed. Figure 2(d) plots the magnetic field on the x–y plane and the induced current loop (red-arrows), indicating the excitation of a resonant magnetic dipole mode. The distribution of the H_z component at the half-height plane of the SRR (which is normalized to the magnetic field intensity of incident light) shows a strong enhancement of the magnetic field mainly confined within the inner area of the SRR, and its corresponding enhancement reaches up to a value of 120.

Figure 3(a) shows the transmittance of our proposed hybrid metamaterials integrating the graphene grating and the SRR together. An evident narrow transparency window at ~8.39 μm is observed for both RCP and LCP excitations. Similar to our previous work, the destructive interference

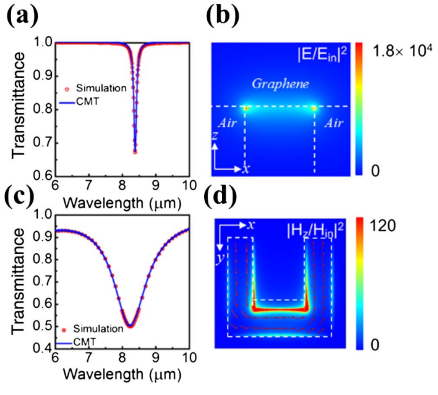

Fig. 2. (a) Transmittance of the graphene grating only. (b) Electric field distribution of the graphene resonator under CPL illumination at the resonance wavelength of 8.45 μm. (c) Transmittance of the SRR array only. (d) Magnetic field distribution at the half-height plane of the SRR under CPL illumination at the resonance wavelength of 8.25 μm.

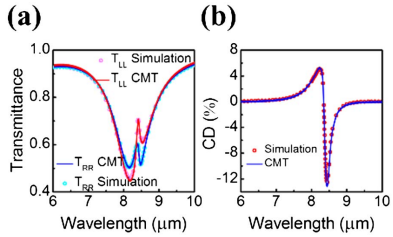

Fig. 3. (a) Transmittance of the hybrid structure for RCP and LCP excitations, and (b) the CD values as a function of wavelength.

between the high-quality factor dipolar resonance mode of the graphene and the low-quality factor magnetic resonance mode of the SRR will lead to the EIT effect [28]. Meanwhile, a prominent transmission intensity difference in the whole transparency window is apparent, indicating a strong CD effect. To quantify the CD effect, the CD value is defined as $(T_{RR} - T_{LL}) \times 100\%$, where T_{RR} (T_{LL}) is the transmittance under the RCP (LCP) light excitation. As shown in Fig. 3(b), the CD value is found to be wavelength dependent within the EIT window, and its maximum is about 13% at the frequency of transmission peak. This value is much higher than what is observed for recent pure graphene chiral metamaterials [25,26]. A slow light effect associated with the EIT [28] can dramatically enhance the light–matter interaction in our hybrid nanostructures, resulting in a strong chiroptical response. The COMSOL simulation results in Figs. 3(a) and 3(b) are in perfect agreement with the analytical calculation based on the CMT. Using the curve-fitting toolbox in Matlab, the CMT parameters used in this Letter are $\gamma_1^s = 0.7393$, $\gamma_1^d = 0.4224$, $\gamma_2^s = 0.0281$, $\gamma_2^d = 0.0495$, and $\kappa = 0.2329$.

Since the symmetry breaking and coupling strengths between the electric and magnetic resonant modes are the key factors in our system, we study separately the impacts of these two factors on the generation of CD. Figures 4(a) and 4(b) show the influence of the structure symmetry on the CD by changing the SRR rotation angles θ. The CD value increases as θ increases from 0° to 45°. The maximum CD value up to 13% is recorded when the θ reaches 45°, corresponding to the largest extent of structure symmetry breaking. Then it decreases with the decreasing of the symmetry breaking and, finally, disappears when the θ changes to 90°. The coupling strength between the graphene strip and the SRR is changed by tuning the efficiency of the EIT-like resonance [28], which is achieved through varying μ from 10,000 to 1000 cm^2/Vs while fixing the rotation angle $\theta = 45°$. As shown in Fig. 4(c), the CD values within the transparency window of the EIT increase monotonously with the increasing of μ, which confirms the beneficial role of the strong plasmonic resonances of graphene nanoribbons [28] in controlling the strength of chirality.

Then we study the electronic tunability of the CD effect in our hybrid structure. As mentioned above, one of the major advantages of graphene compared to noble metals (such as gold and silver) is its active broadband tunability of the Fermi energy (E_f) by electrostatic gating and chemical doping, which opens up a new gateway to achieving continuously tunable chiral elements. Figure 5(a) shows the CD spectra with various graphene Fermi energies. In this simulation, E_f is changed from 0.7 to 0.9 eV, while the other parameters are set as $\theta = 45°$, $\mu = 10{,}000$ cm^2/Vs, $w_g = 230$ nm, and $\varepsilon_d = 1.0$. It is clear

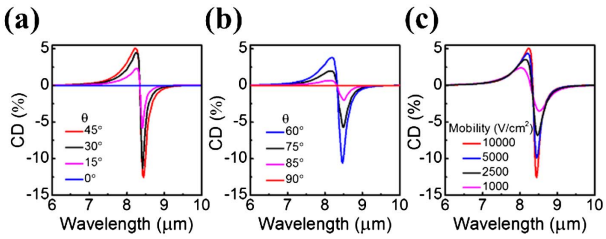

Fig. 4. CD spectra of the hybrid structure with the rotation angle of the SRR varying from (a) 0° to 45° and (b) 60° to 90°. (c) CD spectra with different electronic mobilities of the graphene grating.

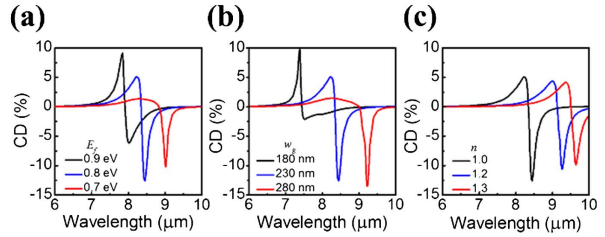

Fig. 5. CD spectra of the hybrid structure with different (a) Fermi energies, (b) widths of graphene strip, and (c) matrix permittivities.

that the CD peak is tunable within a large range and shows an obvious blue-shift as E_f increases.

In addition, the CD effect can also be tuned through changing the structural parameters of the graphene strips. As shown in Fig. 5(b), an obvious red-shift of the CD peak is demonstrated with the width of the graphene strip (w_g) increasing from 180 to 280 nm. This is due to the size dependence of the dipole resonance of the graphene resonator. Here $\theta = 45°$, $\mu = 10{,}000$ cm^2/Vs, $E_f = 0.8$ eV and $\varepsilon_d = 1.0$. Finally, the environmental index offers us another degree of freedom to tune the CD effect of the graphene–metal hybrid metamaterial. Practically, the whole structure could be immersed or embedded in different background dielectrics. Here we assume that the refractive index of the background material changes from 1 to 1.3 with $\theta = 45°$, $\mu = 10{,}000$ cm^2/Vs, $E_f = 0.8$ eV, and $w_g = 230$ nm. The corresponding CD peak exhibits a gradual red-shift as refractive index increases, as shown in Fig. 5(c). This range of refractive index covers the achievable materials, such as ion gel and electro-optic polymers.

In summary, we have numerically studied the mid-infrared CD effect generated by a novel electrically tunable EIT-like metamaterial consisting of a top-layer gold SRR array and a bottom-layer graphene grating. The strong CD reaches the maximum of around 13% when our structure has the largest structure symmetry breaking and strong near-field electromagnetic interaction. The optical chirality is well explained by CMT, fitting the numerical simulations perfectly. Moreover, the CD signals can be dynamically tuned and maintain greater than 10% in a wide wavelength range by varying the Fermi energy of graphene, the geometry parameters, and the refractive index of the matrix material. When applied to specific applications, these parameters should be determined by the spectrum interval of interest. Although the present results are all obtained at normal incidence, we remark that comparable chiroptical response remains at oblique incidence [8]. This study may provide a versatile platform for designing active metadevices with applications in enantiomers identification, analytical chemistry, and molecule sensors.

Funding. National Key R&D Program of China (2017YFA0303702); National Natural Science Foundation of China (NSFC) (11621091, 11674166, 11774162); Office of Naval Research (ONR) (N00014-16-1-2409).

REFERENCES

1. W. T. B. Kelvin, *Baltimore Lectures on Molecular Dynamics and the Wave Theory of Light* (C. J. Clay and Sons, 1904).
2. V. Saranathan, C. O. Osuji, S. G. Mochrie, H. Noh, S. Narayanan, A. Sandy, E. R. Dufresne, and R. O. Prum, Proc. Natl. Acad. Sci. USA **107**, 11676 (2010).
3. V. Sharma, M. Crne, J. O. Park, and M. Srinivasarao, Science **325**, 449 (2009).
4. W. A. Bonner, *Origins of Life and Evolution of Biospheres* (1991), Vol. **21**, p. 59.
5. H. Raether, *Surface Plasmons on Smooth and Rough Surfaces and on Gratings* (Springer-Verlag, 2013).
6. C. Huck, F. Neubrech, J. Vogt, A. Toma, D. Gerbert, J. Katzmann, T. Härtling, and A. Pucci, ACS Nano **8**, 4908 (2014).
7. Y. Tang and A. E. Cohen, Science **332**, 333 (2011).
8. Z. Wang, H. Jia, K. Yao, W. Cai, H. Chen, and Y. Liu, ACS Photonics **3**, 2096 (2016).
9. Z. Wang, L. Jing, K. Yao, Y. Yang, B. Zheng, C. M. Soukoulis, H. Chen, and Y. Liu, Adv. Mater. **29**, 1700412 (2017).
10. Z. Wu and Y. Zheng, Adv. Opt. Mater. **5**, 1700034 (2017).
11. A. Ben-Moshe, A. Teitelboim, D. Oron, and G. Markovich, Nano Lett. **16**, 7467 (2016).
12. H. H. Brintzinger, D. Fischer, R. Mülhaupt, B. Rieger, and R. M. Waymouth, Angew. Chem. Int. Ed. **34**, 1143 (1995).
13. W. Chen, D. C. Abeysinghe, R. L. Nelson, and Q. Zhan, Nano Lett. **10**, 2075 (2010).
14. I. Goykhman, B. Desiatov, J. Khurgin, J. Shappir, and U. Levy, Opt. Express **20**, 28594 (2012).
15. Z. Fan and A. O. Govorov, J. Phys. Chem. C **115**, 13254 (2011).
16. S. Yuan, R. Roldán, A.-P. Jauho, and M. Katsnelson, Phys. Rev. B **87**, 085430 (2013).
17. J. A. Fürst, J. G. Pedersen, C. Flindt, N. A. Mortensen, M. Brandbyge, T. G. Pedersen, and A. P. Jauho, New J. Phys. **11**, 095020 (2009).
18. V. Singh, D. Joung, L. Zhai, S. Das, S. I. Khondaker, and S. Seal, Prog. Mater. Sci. **56**, 1178 (2011).
19. W. B. Lu, W. Zhu, H. J. Xu, Z. H. Ni, Z. G. Dong, and T. J. Cui, Opt. Express **21**, 10475 (2013).
20. A. Vakil and N. Engheta, Science **332**, 1291 (2011).
21. S. Thongrattanasiri, F. H. Koppens, and F. J. Garcia de Abajo, Phys. Rev. Lett. **108**, 047401 (2012).
22. W. Zhu, I. D. Rukhlenko, L.-M. Si, and M. Premaratne, Appl. Phys. Lett. **102**, 121911 (2013).
23. P. Weis, J. L. Garcia-Pomar, M. Höh, B. Reinhard, A. Brodyanski, and M. Rahm, ACS Nano **6**, 9118 (2012).
24. Z. Wu, W. Li, M. N. Yogeesh, S. Jung, A. L. Lee, K. McNicholas, A. Briggs, S. R. Bank, M. A. Belkin, D. Akinwande, and Y. Zheng, Adv. Opt. Mater. **4**, 2035 (2016).
25. X. T. Kong, R. Zhao, Z. Wang, and A. O. Govorov, Nano Lett. **17**, 5099 (2017).
26. T. Wang, Y. Wang, L. Luo, L. Wang, and Z. Zhang, Plasmonics **12**, 829 (2017).
27. T. Cao, C. W. Wei, L.-B. Mao, and S. Wang, Opt. Express **23**, 18620 (2015).
28. Z. Huang, Y. Dai, G. Su, Z. Yan, P. Zhan, F. Liu, and Z. Wang, Plasmonics **13**, 451 (2018).
29. N. Liu, L. Langguth, T. Weiss, J. Kästel, M. Fleischhauer, T. Pfau, and H. Giessen, Nat. Mater. **8**, 758 (2009).
30. M. Kang and Y. D. Chong, Phys. Rev. A **92**, 043826 (2015).